Fall 2021

Oblique Shock Wave Diffuser Design

Noah Riggenbach
ndr21@uakron.edu

Oblique Shock Wave Diffuser Design

Noah Riggenbach

Fall 2021

Table of Contents

I. Abstract

In this Honors Research Project, I will investigate the aerodynamic drag on certain defined ramps and cone/cylinder geometries representing oblique shock wave diffusers. The goal is to develop an oblique shock wave diffuser that decelerates supersonic air while maintaining a limited aerodynamic drag profile. The aerodynamic drag will first be obtained by calculating the pressure coefficient and the skin friction coefficient using the fluid simulation software ANSYS Fluent (version 2019). Limiting drag is important for aircraft flight performance, especially at supersonic speeds. At flight speeds above Mach 1, shock waves form and the air passing through these waves experiences a dramatic increase in pressure, density and temperature. For proper function of air-breathing supersonic aircraft engines, supersonic air must be decelerated to subsonic flow in a diffuser or the shock waves will cause damage to the engines. Oblique shock waves create less stagnation pressure loss than normal shock waves, which allows for increased flight performance. This research will deepen our understanding of how the design of oblique shock wave diffusers affects drag.

II. Acknowledgements

I would like to thank Dr. Povitsky for guiding me through this project. Especially because of the new software learning curve and meeting entirely online during the spring because of COVID-19. I couldn't have done it without him. Also, thanks to Dr. Daniels, Dr. Buldum, and Dr. Quinn for proofing and suggestions.

III. Background

For the proper operation of supersonic jet engines, it is necessary that air be decelerated to subsonic speed. Air transitioning from supersonic to subsonic speed passes through a shock wave. A shock wave is a very thin region in which lower pressure, lower temperature, and supersonic fluid experiences a drastic change to higher pressure, higher temperature, and low velocity.[1] If this occurs in the fan or compressor of a jet engine, or even at a later stage, the engine will be significantly damaged. Therefore, it is essential that this deceleration take place before the compressor, usually in a diffuser.

Aircraft performance is greatly impacted by the characteristics of the diffuser, and diffuser optimization is the main focus of this study. Under the adiabatic assumption, air passing through a shock wave will maintain the same stagnation temperature while undergoing a decrease in stagnation pressure. A normal shock wave is perpendicular to the direction of flow. An oblique shock wave is at an arbitrary angle to the direction of flow.[2] As a part of stagnation pressure losses across shock waves, viscous boundary layers are another important aspect to optimizing diffuser efficiency. Because of fluid viscosity, a boundary layer is created to bridge the gap between fluid flowing at a large free stream velocity and fluid at a no slip boundary condition at a wall.[3] Interactions between shock waves and boundary layers can create recirculation zones, areas in which fluid flow direction is counter to main body flow.[4] Recirculation zones negatively impact aerodynamic performance as detailed below.

By understanding the interaction between shock waves and boundary layers, it is the goal of this research project to be able to design more efficient diffusers. This report will build on the work of previous honors projects by Fulop, Henry, Ruffner, and McMullen in *Supersonic Propulsion: Inlet Shock Wave/Boundary Layer Interaction in a Diffuser* and Keuchel, Andrews, and Rahe in *Shock Wave and Boundary Layer Interaction.*

Keuchel et. al summarized the use of the two major shape designs used for diffusers. Cones extend in front of the main diffuser passage in which shock waves are directed. Then ramp designs produce several oblique shockwaves so that air is decelerated and the static pressure is increased.[5] Keuchel et. al examined the properties of single

ramps, double ramps, and curved ramps. Their goal was to evaluate diffuser efficiency by determining the loss of stagnation pressure and the contribution of skin friction drag which indicates the effect of shock wave boundary layer interactions. Keuchel's group varied the length, angle, and position of the ramps to determine ideal geometries. Fulop et. al also looked at single and double ramp geometries with a variety of angles. Keuchel and Fulop used the same methods to determine efficiency.[6] See Figure 1 below.

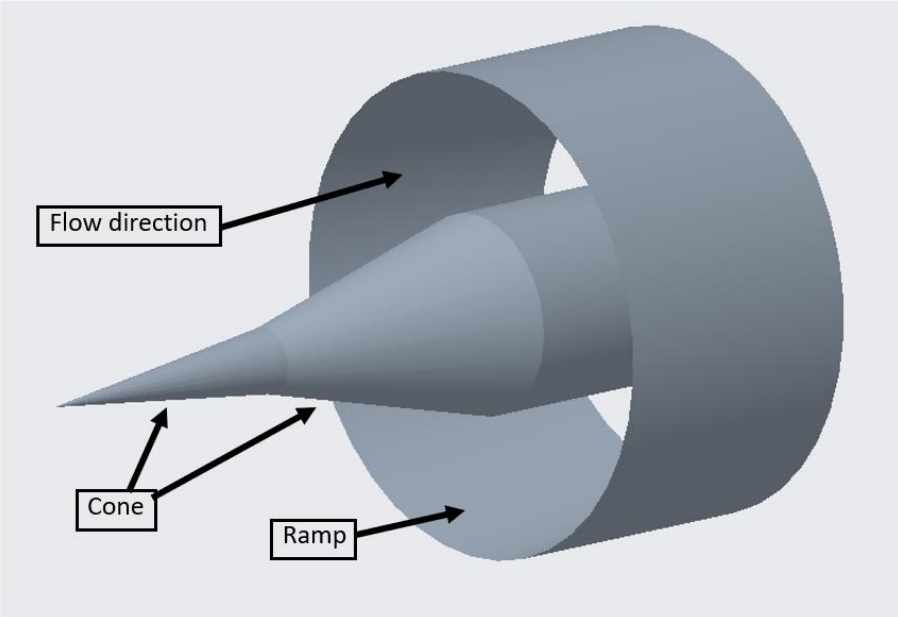

Figure 1: Cone and Ramp Diffuser

Keuchel et. al found that oblique shock waves were less defined at greater Mach speeds and that the size of the shock wave was proportional to the angle of the ramp (larger angles led to larger shock waves), which has been experimentally proven.[7] They also discovered that greater ramp angles led to larger stagnation pressure losses, and interestingly, that the ramp angle does not affect the skin friction coefficient.[8]

Keuchel et al. concluded that double ramps produced greater deceleration and kept stagnation pressure loss close to the ramp walls. For the curved ramp it was determined that increasing Mach speed led to a decreased oblique shock wave angle while increasing the curved ramp angle led a more significant fluid deceleration and a greater drop in stagnation pressure.[9]

Keuchel's group concluded that diffusers designed to create normal shock waves are less efficient than diffusers designed to create oblique shock waves because they created large recirculation zones due to boundary layer separation. Their best design was a 20° double ramp with a 0.4m channel with 8.56% stagnation pressure loss.[10]

However, one big problem with Andrew's design was that it failed to completely decelerate the air in the channel to below Mach 1. Some pockets of air flow were subsonic, but not all. The remaining supersonic airflow would be enough to damage the compressor or fan of the jet, thereby rendering the diffuser ineffective. It is the goal of this project to design a diffuser that completely decelerates the air to subsonic speeds and maximizes efficiency using Fulop's and Andrew's research into shock wave and boundary layer interaction.

IV. Modeling, Simulation, and Procedure

Each diffuser design was evaluated with ANSYS Fluent 2019, the same software version as both Keuchel and Folup, in a workbench module. Three Fluent solver models were used including the Spalart-Allmaras, Inviscid, and LES models. The Spalart-Allmaras is a one equation version of the of the Navier-Stokes equations which makes it easier to solve. It is a Reynolds-averaged Navier Stokes model which means that it outputs the averages of turbulent eddies over time even though a true picture of the flow at an instant in time will be different because of the unsteady variations in flow.[11] It was the model used primarily in this study. The inviscid model assumes that there is no viscosity so any pressure losses due to boundary layer interactions are neglected. The LES model is based upon the fact that turbulent flows contain eddies, and these eddies need to be resolved with a fine mesh. Four meshing cells are needed to resolve an eddy, although a sub grid scale model can be used for eddies that are smaller than our mesh size.[12] Therefore, the fineness of the mesh determines the minimum eddy size that can be resolved. Based upon the Turbulent Energy Cascade, a good LES model will resolve 80% of turbulent kinetic energy.[13] Each specific diffuser design was drawn in Design Modeler, then meshed. Each diffuser was modelled with a structured, quadrilateral mesh; see Figure 2 below.

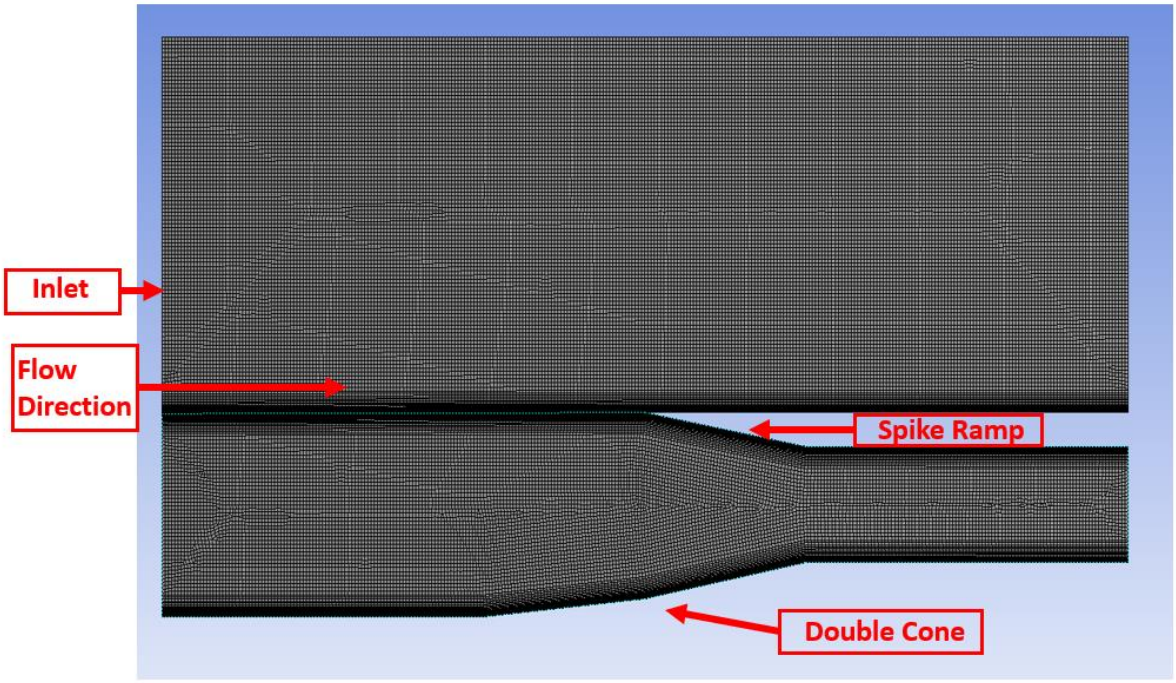

Figure 2: Overview of Structured Mesh

Background element size was defined with edges of 0.01 m. The mesh included an inflation layer, a region with a highly detailed grid, near the walls of the diffuser. Inflation layers are needed to capture boundary layer detail. The mesh used in this report's simulations stretched the inflation layer from the spike tip horizontally to the inlet by dividing the domain into two subdomains. This allows for a structured mesh at the tip of the upper diffuser spike. The structured inflation layer at this point is especially important for solver robustness and the accuracy of the simulation results. The inflation layer was defined by the total number of layers (20), seed height (0.001 m), and growth rate (1.1). The seed height sets the height of the inflation layer nearest the wall, and the growth rate determines the ratio between adjacent layers. See Figure 3 below.

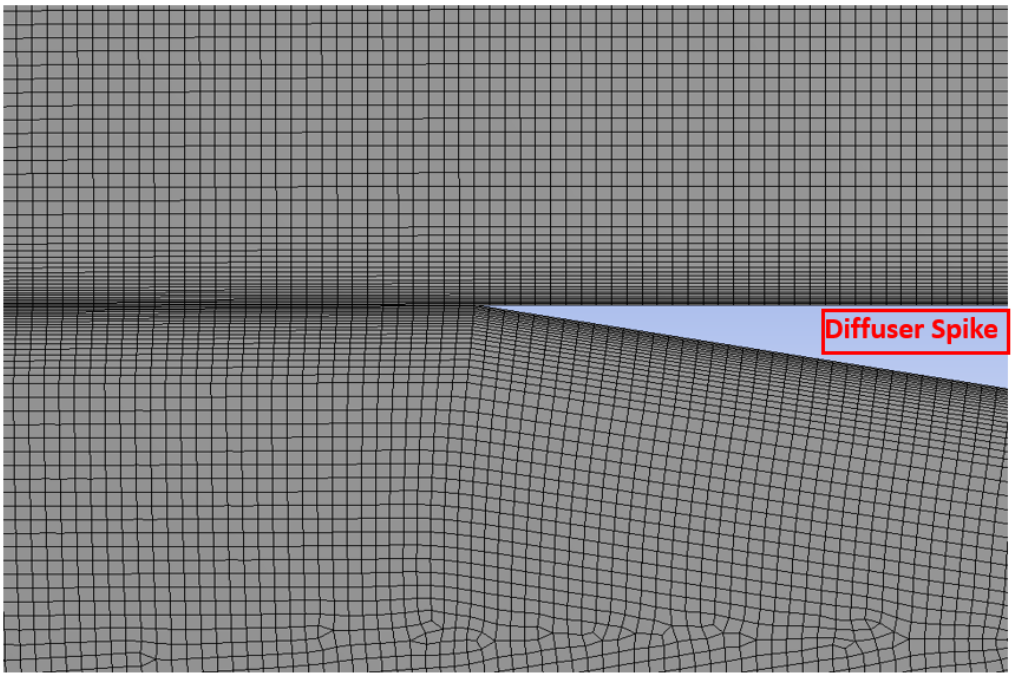

Figure 3: Structured Mesh at Spike Geometry

Compare the structured mesh at the tip in Figure 3 with the unstructured meshes in Figures 4, 5, and 6. Their meshes are not structured around the nose of the diffuser spike and at the ramps, likely resulting in large calculation errors. To accurately evaluate their diffuser's performance, their designs were re-simulated.

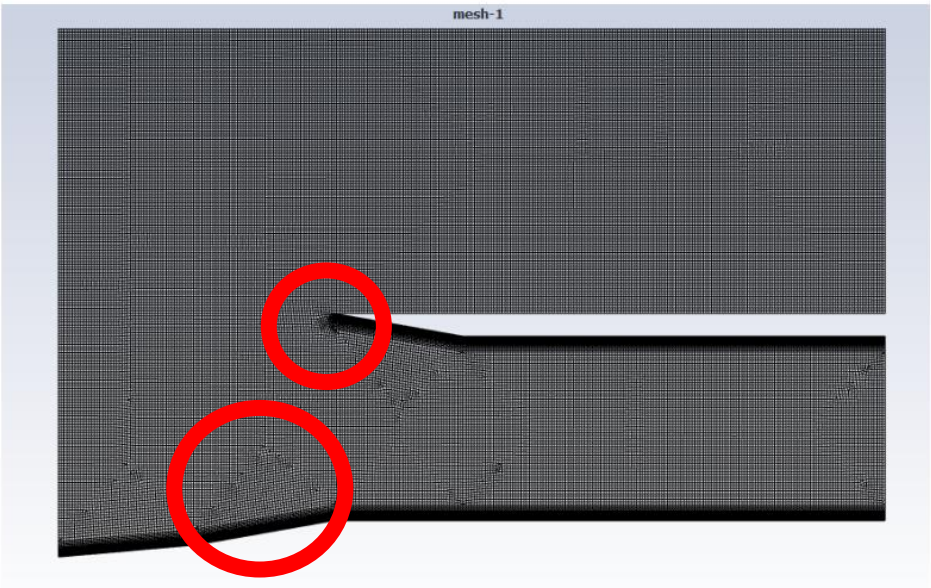

Figure 4: Keuchel's group's mesh with marked irregularities

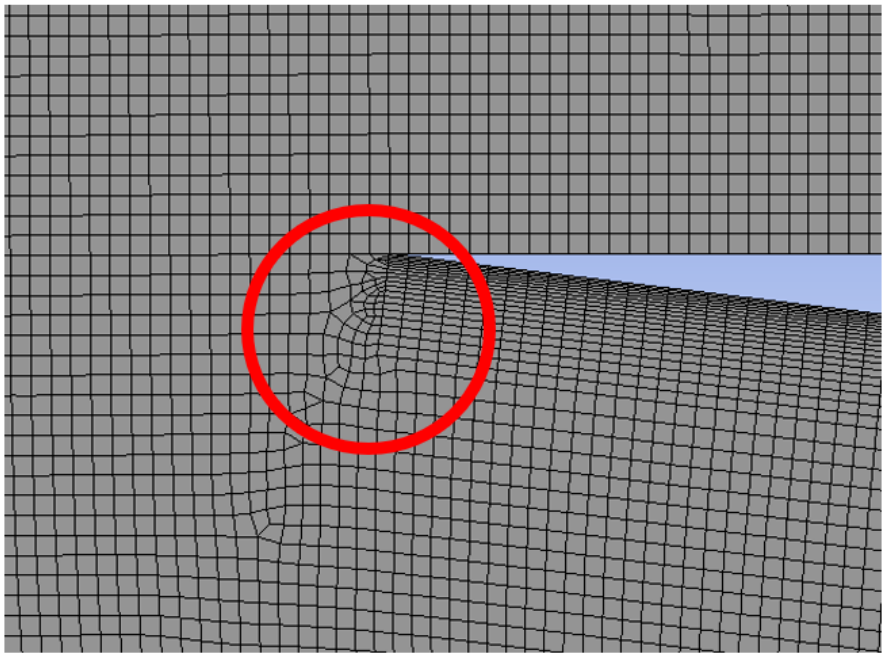

Figure 5: Inset view of the spike tip of Figure 4,

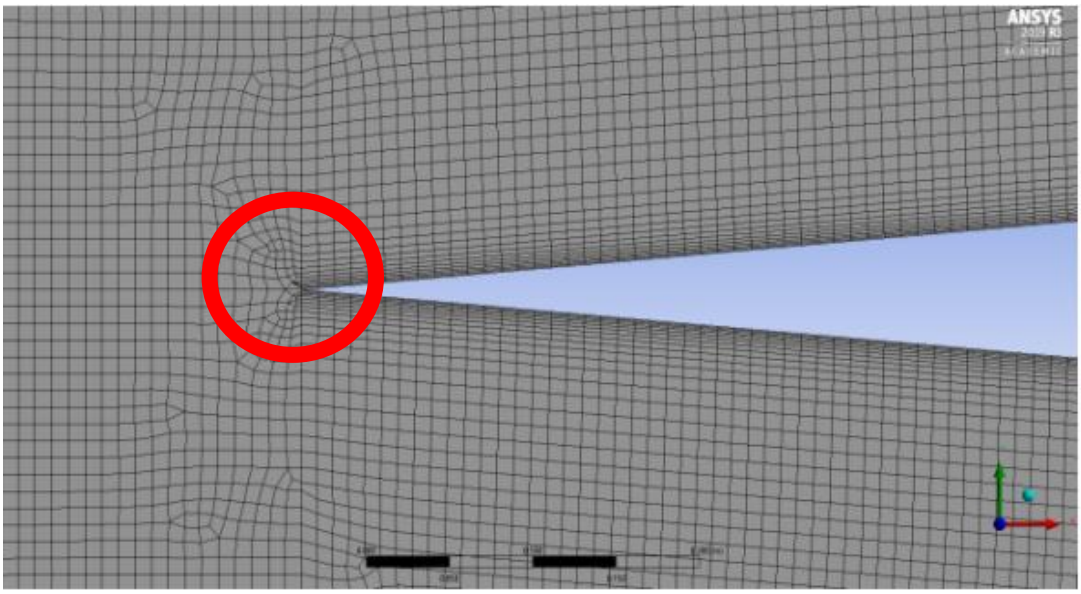

Figure 6: Folup's group's mesh with marked irregularities

Once each diffuser was meshed, named selections were created to define boundary conditions. There is an inlet corresponding to the left edge of the model (red), an upper outlet at the right edge of the model above the diffuser (orange), diffuser outlet (yellow),

the diffuser itself (green), and finally, the air boundary designating the upper and lower edges that are not contained as part of the diffuser geometry (blue) . See Figure 7.

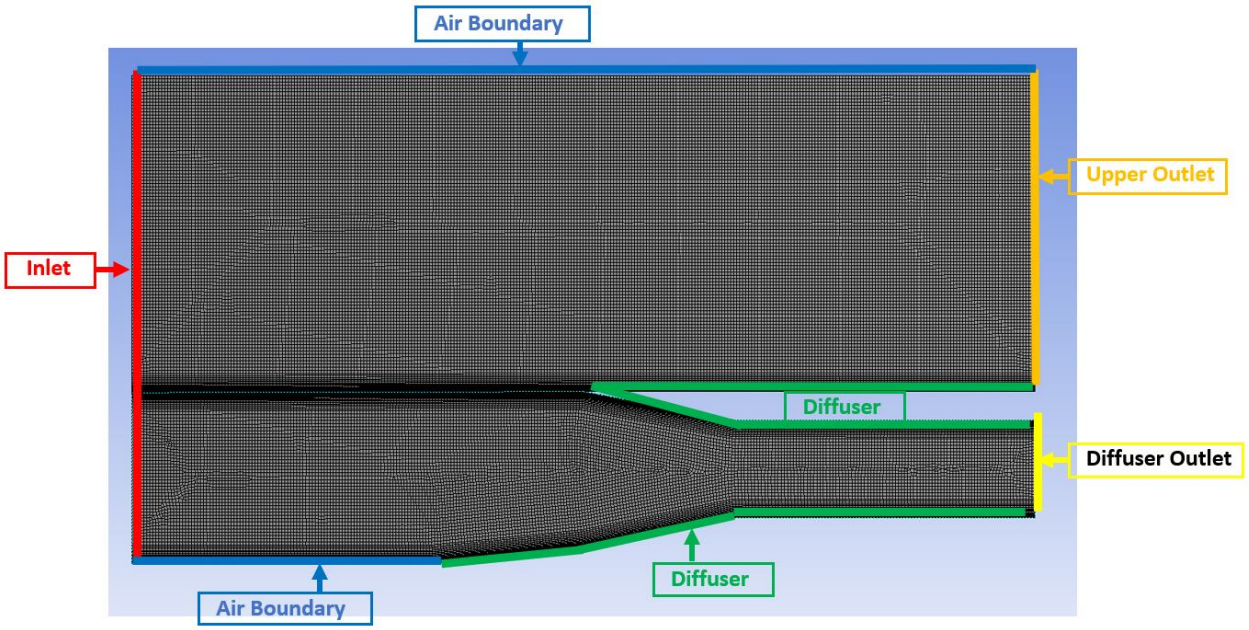

Figure 7: Named Selection Definition

The inlet was defined as a pressure inlet with zero static pressure, 300 K temperature, and an inlet speed of Mach 2 in the x direction. The air boundary was designated a pressure-far-field with zero static pressure 300 K temperature, and a boundary speed of Mach 2 in the x direction. Each outlet was defined as a pressure outlet. The diffuser walls were defined as having zero heat flux.

Each model was given substantial iterations to reach residuals of less than 0.01, corresponding to less than 1% error. The one equation Spalart-Allmaras turbulence model was used in conjunction with the pressure-based solver. The pressure-based solver resulted in better residual convergence, so it was used in all models for consistency. The ideal gas model was also used to define the air instead of a constant density alternate.

Efficiency was evaluated by calculating the drop in stagnation pressure between the inlet and the outlet of each diffuser. High outlet pressure or a lower pressure drop from the inlet is desirable. Contours of stagnation pressure and Mach number were made for each model, along with a plot of the skin friction to examine the impact of recirculation

zones. The results of Keuchel's group were used as a starting point for this investigation. Their results are tabularized in Table 1 below.

Table 1: Andrew's Group Results[14]

Model	Figure #	Total Pressure at Inlet (Pa)	Total Pressure at Outlet (Pa)	Loss of Total Pressure (Pa)	Percent change in pressure
10° 0.65m channel	22	691316.59	622951.98	68364.62	9.89
10° 0.4m channel	26	691316.36	546166.79	145149.57	20.99
10° 0.65m channel	29	691316.44	631899.65	59416.79	8.59
10° 0.4m channel	32	691316.36	631281.99	60034.37	8.68
10° 0.3m channel	35	691316.44	478350.93	212965.51	30.81
16° 0.3m channel	40	632429.38	468881.95	163547.43	25.86
16° 0.5m channel	46	691316.39	608507.23	82809.17	11.98
20° 0.5m channel	52	691316.62	620479.65	70836.97	10.25
20° 0.4m channel	56	691316.54	632137.47	59179.07	8.56
20° 0.3m channel	60	691316.54	468788.38	222528.16	32.19

They found that a configuration with a 20° ramp angle and a 0.4 m channel was the most efficient with 8.56% pressure drop, however their design did not completely decelerate the air to subsonic flow. In this study, the effect of changing the geometry of the double cone and spike ramp were examined to determine the best diffuser design

V. Results

The tabulated results can be found in Table 2 below. The goal is to have the least drop in stagnation pressure. Efficiency is calculated by dividing diffuser outlet stagnation pressure by the inlet stagnation pressure. Diffuser geometry notation used in Table 2 is shown in Figure 8 below. The 1st cone angle is the first angle of the double cone of the diffuser that first contacts the flow. The 2nd cone angle is the second angle of the double cone. The spike ramp angle is the angle of the ramp of the spike geometry. The spike x-position calls out the horizontal component of the distance between the cone tip and the spike tip. For reference, the horizontal length of the double cone is 1 m. The channel depth is the height of the diffuser outlet. See Figure 8 below.

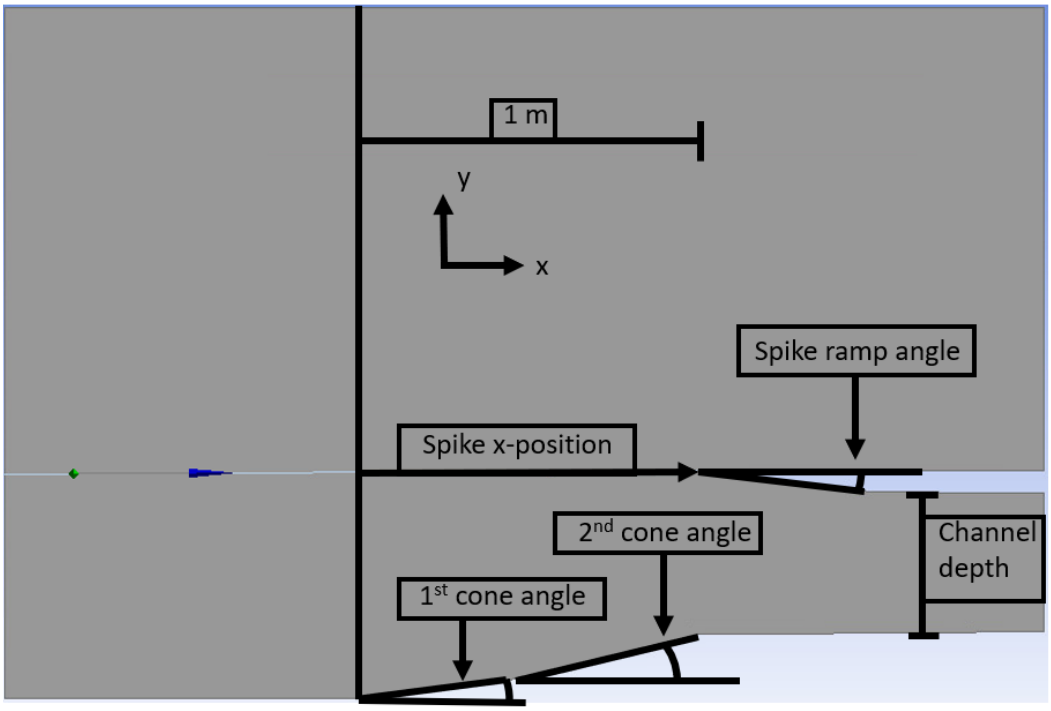

Figure 8: Diffuser Geometry Notation

Table 2: Diffuser Efficiency Results

1st Cone Angle	2nd Cone Angle	Spike Ramp Angle	Channel Depth	Spike x-position	Stagnation Pressure Drop	Efficiency	Diffuser Outlet Mach Number
5	10	10	0.65	1	139617	79.80%	1.024
5	10	10	0.4	1	121817	82.38%	0.894
5	10	10	0.65	0.5	41317	94.02%	1.514
5	10	10	0.4	0.5	193117	72.07%	0.864
5	10	10	0.3	0.5	202017	70.78%	0.830
8	16	10	0.3	0.5	213617	69.10%	0.799
8	16	10	0.5	0.5	221517	67.96%	0.804
10	20	10	0.5	0.5	224117	67.58%	0.766
10	20	10	0.4	0.5	225817	67.34%	0.733
10	20	10	0.3	0.5	226017	67.31%	0.785
5	10	10	0.4	0.9	133217	80.73%	0.875
5	10	10	0.4	1.1	112317	83.75%	0.918
5	10	10	0.4	1.2	99617	85.59%	1.04
3	6	10	0.3	1	127117	81.61%	0.937
4	8	10	0.4	0.75	142117	79.44%	1.200
4	8	10	0.3	0.5	176117	74.52%	0.831
4	8	10	0.4	0.75	142117	79.44%	0.890
5	10	0	0.4	0.5	29967	95.67%	1.519
10	20	12	0.4	0.5	212517	69.26%	0.759
10	20	0	0.3	0.5	225217	67.42%	0.81
10	20	0	0.4	0.5	221317	67.99%	0.823
10	20	0	0.5	0.5	219917	68.19%	0.841
7	14	7	0.4	0.5	213517	69.11%	0.764
7	14	7	0.4	0.75	132317	80.86%	0.764
7	14	7	0.4	1	85967	87.56%	0.900
6	12	6	0.4	1	97917	85.84%	0.977

From Table 2 we can conclude that the best diffuser had a 7° first cone angle, a 14° second cone angle, a 7° spike ramp angle, and a channel depth of 0.4 m. This diffuser had an efficiency of 87.5 %. See Figure 9 for the Mach Number contour for this diffuser.

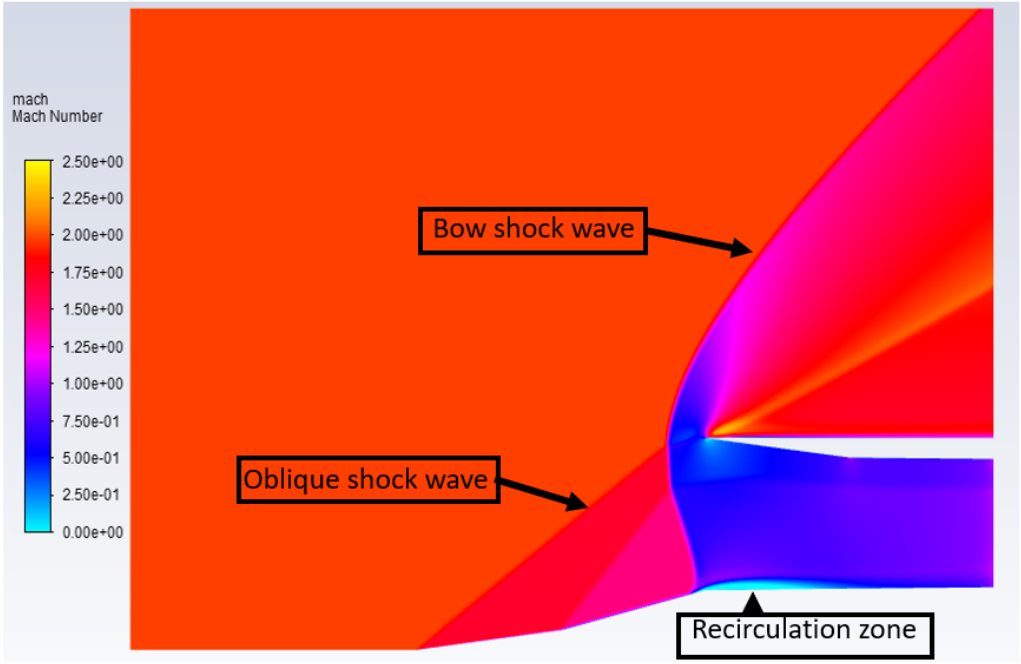

Figure 9: Mach Number contour of 7° 1st cone angle, 14° 2nd cone angle, 7° spike ramp angle, 0.4 m channel depth, 1 m spike position

Note the weak detached bow shock wave and the small recirculation zone below the spike ramp (light blue). See Figure 10 below for a contour of stagnation pressure.

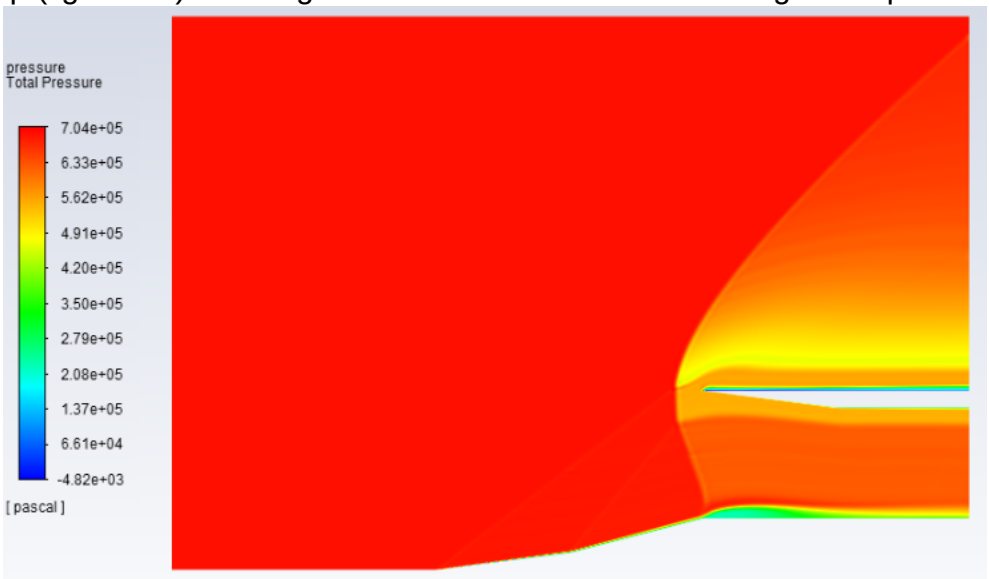

Figure 10: Stagnation Pressure contour of 7° 1st cone angle, 14° 2nd cone angle, 7° spike ramp angle, 0.4 m channel depth, 1 m spike position

Figure 11, below, is the skin friction coefficient plot of the diffuser walls. Position at 1 m horizontally corresponds to the start of the double cone (lower wall - black) and position at 2 m horizontally corresponds to the start of the spike geometry (upper wall - red).

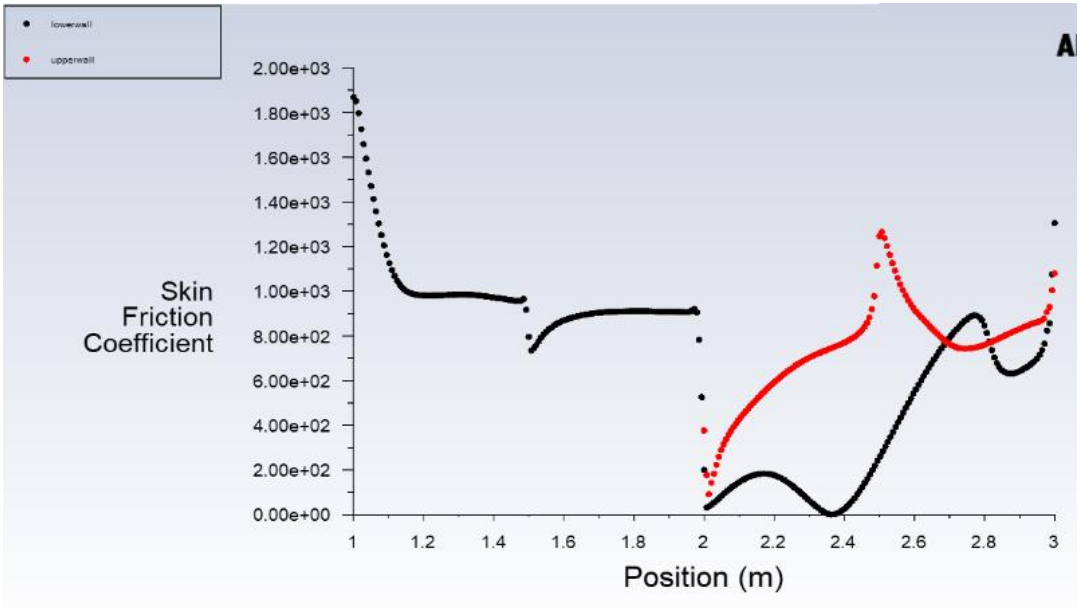

Figure 11: Skin Friction Coefficient of 7° 1st cone angle, 14° 2nd cone angle, 7° spike ramp angle, 0.4 m channel depth, 1 m spike position

Note the low values of the skin friction coefficient for the lower wall (black) between 2 and 2.4 m. This corresponds to the recirculation zone visible in Figure 9. To see the differences between an efficient and inefficient diffuser design, consider Figures 12-14 for the 5° 1st cone angle, 10° 2nd cone angle, 10° spike ramp angle, 0.3 m channel depth, 0.5 m spike position diffuser which has an efficiency of 70.8%.

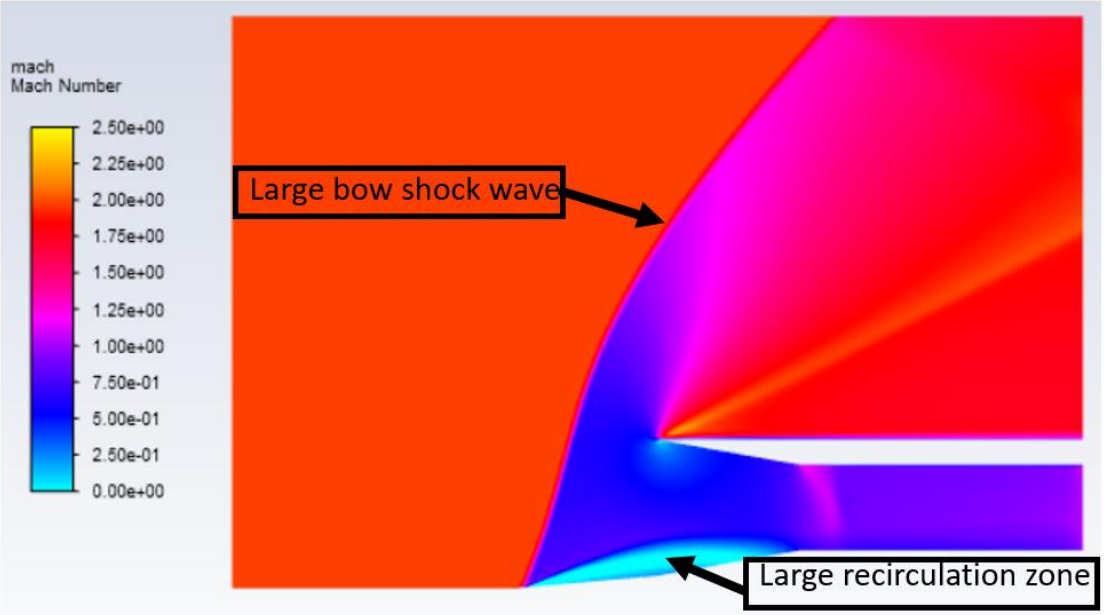

Figure 12: Mach Number contour of 5° 1st cone angle, 10° 2nd cone angle, 10° spike ramp angle, 0.3 m channel depth, 0.5 m spike position

When compared with Figure 7, the large detached bow wave and huge recirculation zone are apparent. Both of these factors contribute to the inefficiencies of this design.

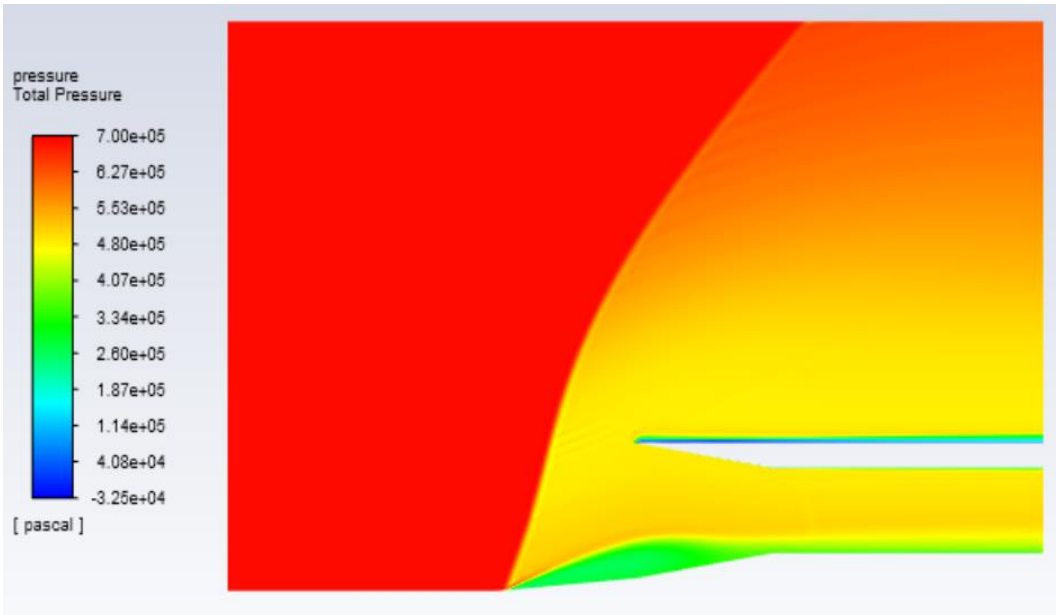

Figure 13: Stagnation Pressure contour of 5° 1st cone angle, 10° 2nd cone angle, 10° spike ramp angle, 0.3 m channel depth, 0.5 m spike position

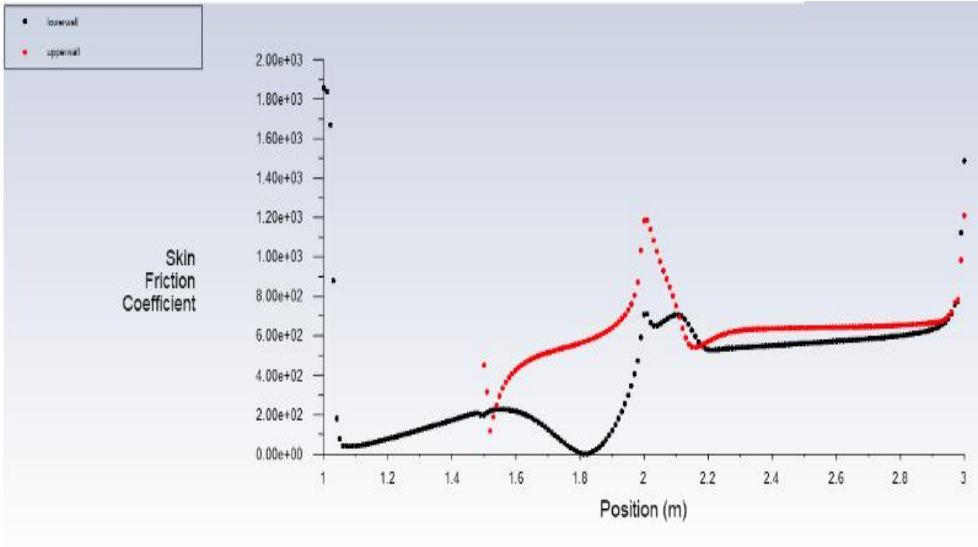

Figure 14: Skin Friction coefficient of 5° 1st cone angle, 10° 2nd cone angle, 10° spike ramp angle, 0.3 m channel depth, 0.5 m spike position

VI. Analysis

When diffuser efficiency is plotted vs the Mach Number in the diffuser outlet, this suggests that the closer the final Mach number is to 1, the more efficient the diffuser; see Figure 15.

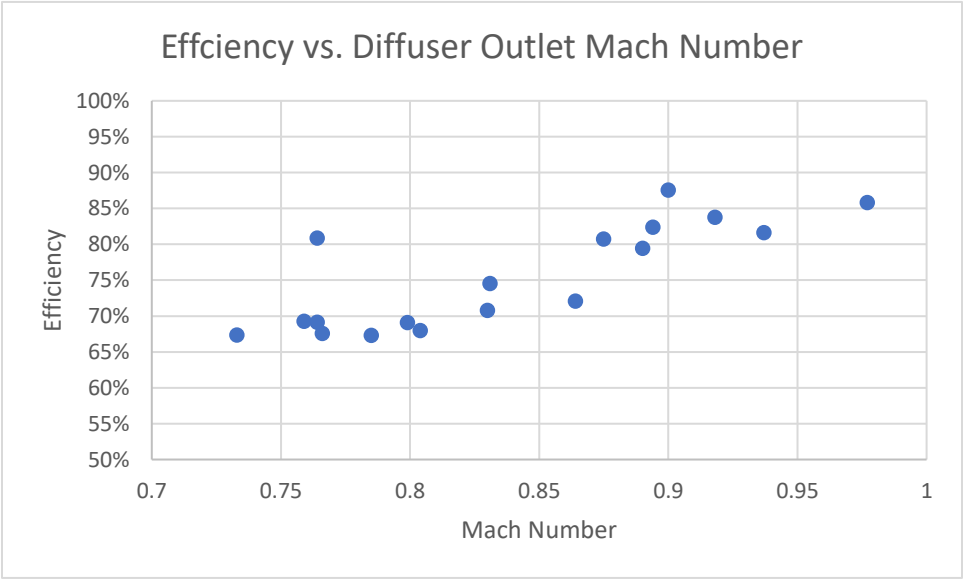

Figure 15: Diffuser Efficiency vs Diffuser Outlet Mach Number

Therefore, when designing a diffuser for a specific Mach number, care should be taken to keep the final Mach number as close as possible to 1. Practically, this means that a fixed diffuser design should be designed to just bring flow to subsonic speeds for the associated aircraft's max speed. For a diffuser with movable inlets, the ramps should be adjusted so that the final airspeed is just below Mach 1 for all Mach input flows.

From theory, increasing ramp angles leads to stronger shock waves that lead to greater drops in stagnation pressure and drops in Mach number. Optimization of ramp angle steepness is the best way to design an efficient diffuser.

In addition to ramp angles' steepness, positioning the ramp to maximize oblique shock wave interaction also impacts efficiency. Ramp positioning also impacts the size and location of the recirculation zone. Compare Figures 16 and 17, which have the same cone and spike angles and diffuser height, but different positioning of the spike.

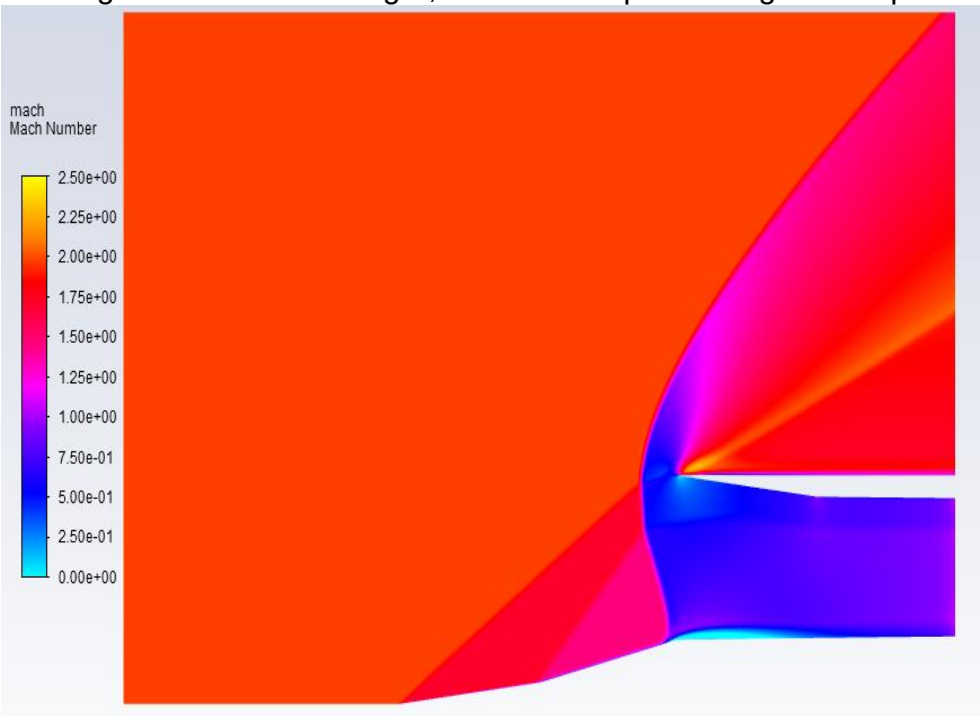

Figure 16: Mach Number contour of 7° 1st cone angle, 14° 2nd cone angle, 7° spike ramp angle, 0.4 m channel depth, 1 m spike position

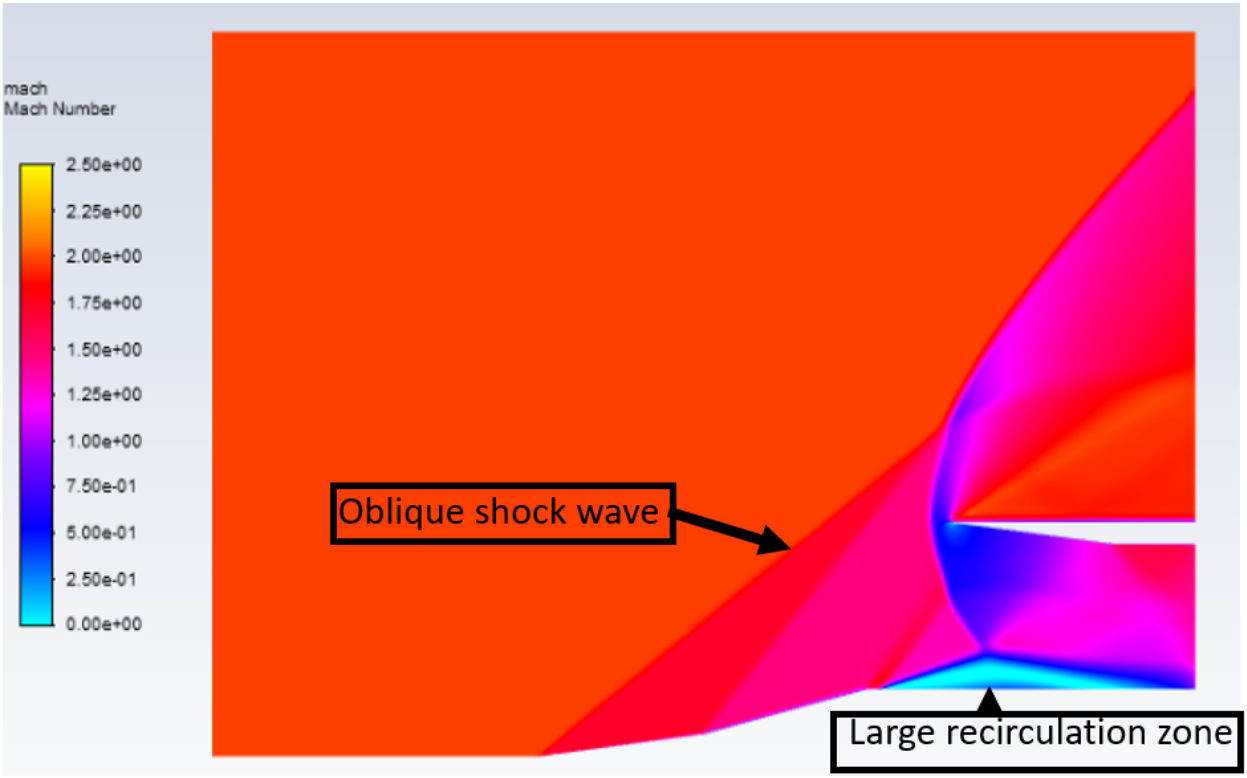

Figure 17: Mach Number contour of 7° 1st cone angle, 14° 2nd cone angle, 7° spike ramp angle, 0.4 m channel depth, 1.25 m spike position

The diffuser with the spike set 0.25 m to the right does not have enough oblique shock wave interaction and fails to successfully decelerate the airflow. It is also inefficient with a massive recirculation zone.

To examine the impact of skin friction on efficiency, the Spalart Model was compared to the inviscid model. The most successful diffuser was 87.56% efficient with a stagnation pressure loss of 86.0 kPa. Using the inviscid model, which does not include viscous effects, the pressure drop was 77.9 kPa. Therefore, we can conclude that skin friction accounts for roughly 10% of efficiency loss for this diffuser. See Figure 18, and note that it is very similar to the Spalart model (Figure 10).

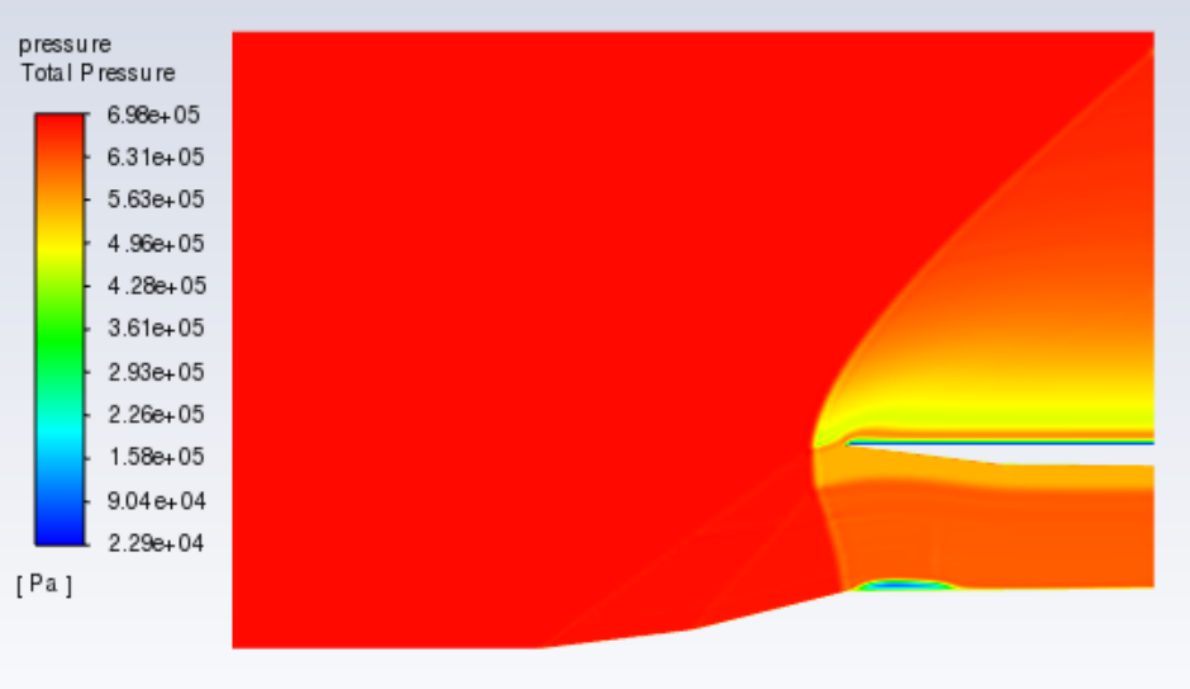

Figure 18: Mach Number contour of 7° 1st cone angle, 14° 2nd cone angle, 7° spike ramp angle, 0.4 m channel depth, 1.25 m spike position

Finally, the most successful diffuser was examined with a Large Eddy Simulation solver to compare it to the Spalart-Allmaras model. The LES simulation for the 7° 1st cone angle, 14° 2nd cone angle, 7° spike ramp angle, 0.4 m channel depth, 1 m spike position diffuser resulted in a Mach number of 0.947 before the channel, but the recirculation zone acted as a diverging nozzle accelerating the air above Mach 1 in the channel. Stagnation pressure loss was 87 kPa, resulting in 87.4% efficiency. The Spalart model resulted in a Mach number of 0.900 and 87.6% efficiency. The efficiency result is very similar; however, the decelerated Mach number is around 5% different between the

differing models. See Figures 19 and 20 for contours of Total Pressure and Mach Number.

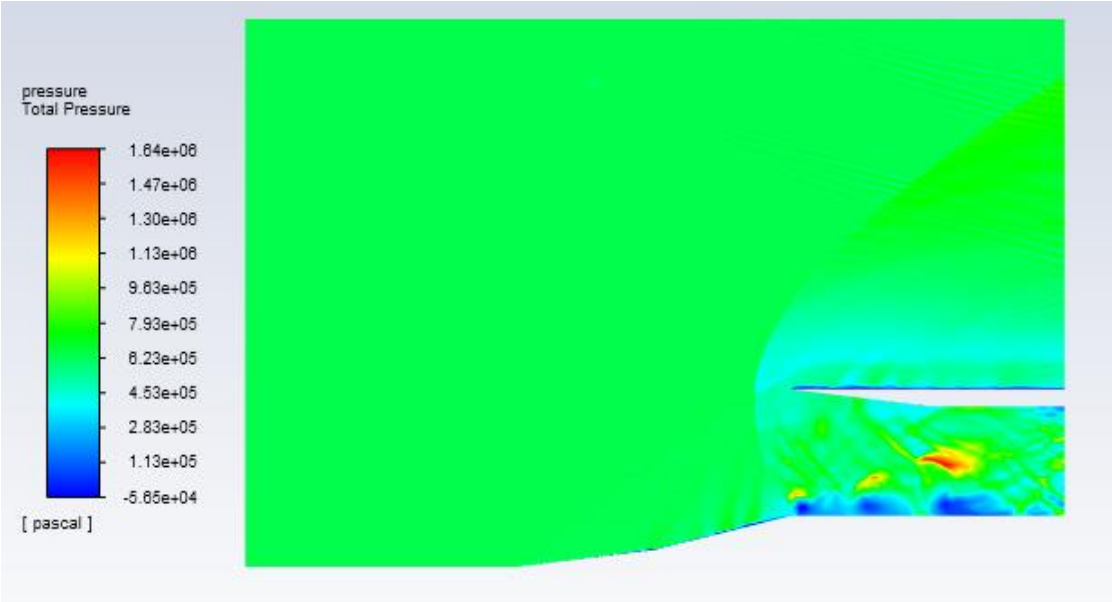

Figure 19: LES Total Pressure for 7° 1st cone angle, 14° 2nd cone angle, 7° spike ramp angle, 0.4 m channel depth, 1 m spike position

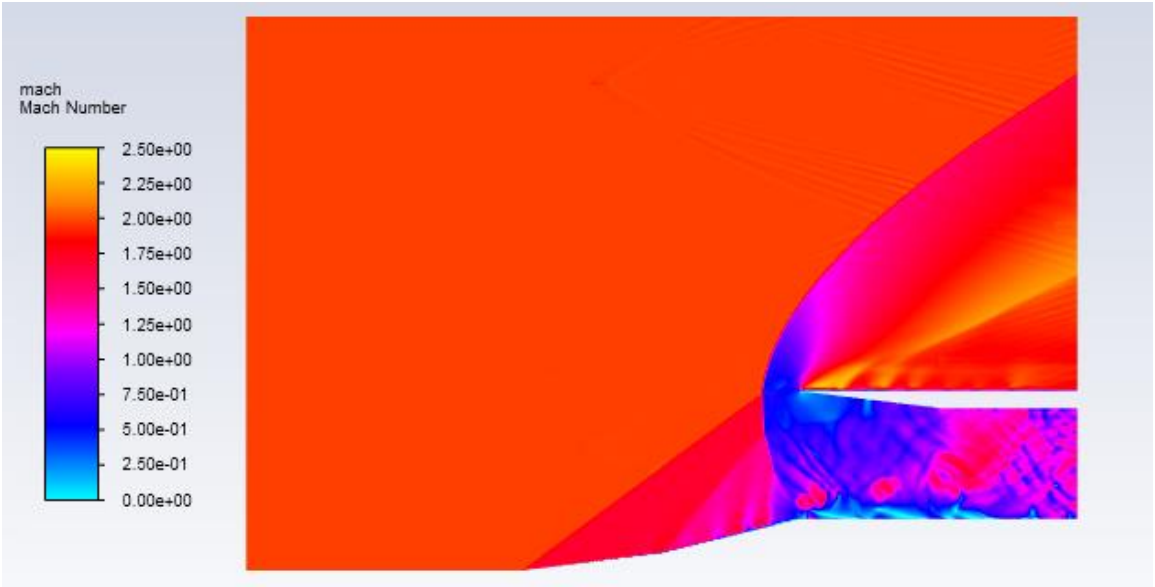

Figure 20: LES Mach Number for the 7° 1st cone angle, 14° 2nd cone angle, 7° spike ramp angle, 0.4 m channel depth, 1 m spike position

A comparison of the size of the recirculation zones of the LES and Spalart models found that the LES recirculation zone was 2.4 times bigger by area; see Figures 21 and 22.

The size of the LES recirculation zone was 0.6 m in the x-direction and 0.2 m in the y-direction. The size of the Spalart recirculation zone was 0.5 m in the x-direction and 0.1 m in the y-direction. Figure 21 shows that there are three smaller eddies that make up one large recirculation zone for the LES model. Figure 22 shows one eddy that makes up the Spalart recirculation zone.

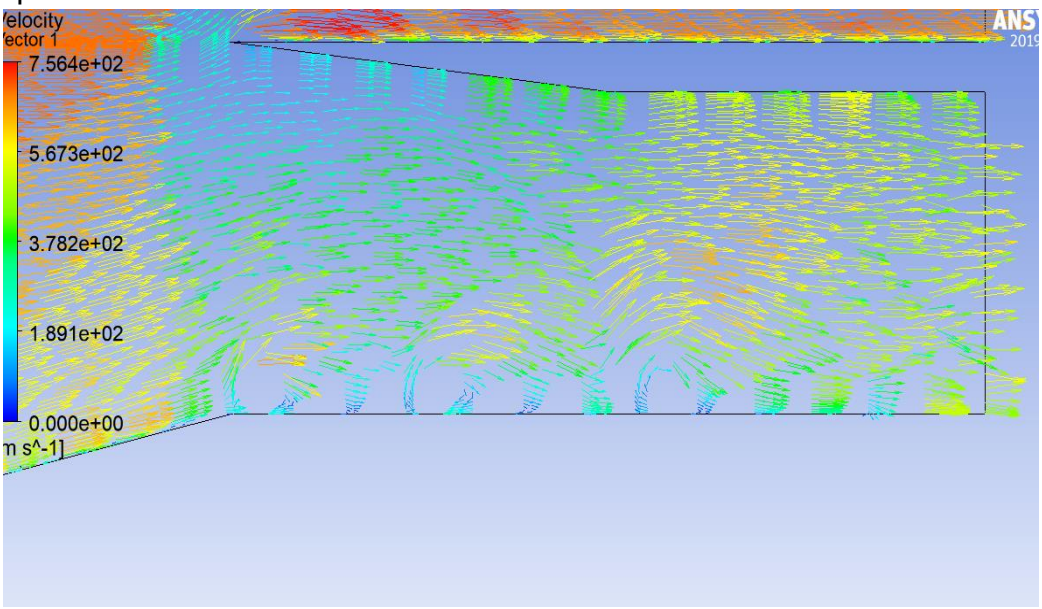

Figure 21: LES Recirculation Zone for the 7° 1st cone angle, 14° 2nd cone angle, 7° spike ramp angle, 0.4 m channel depth, 1 m spike position

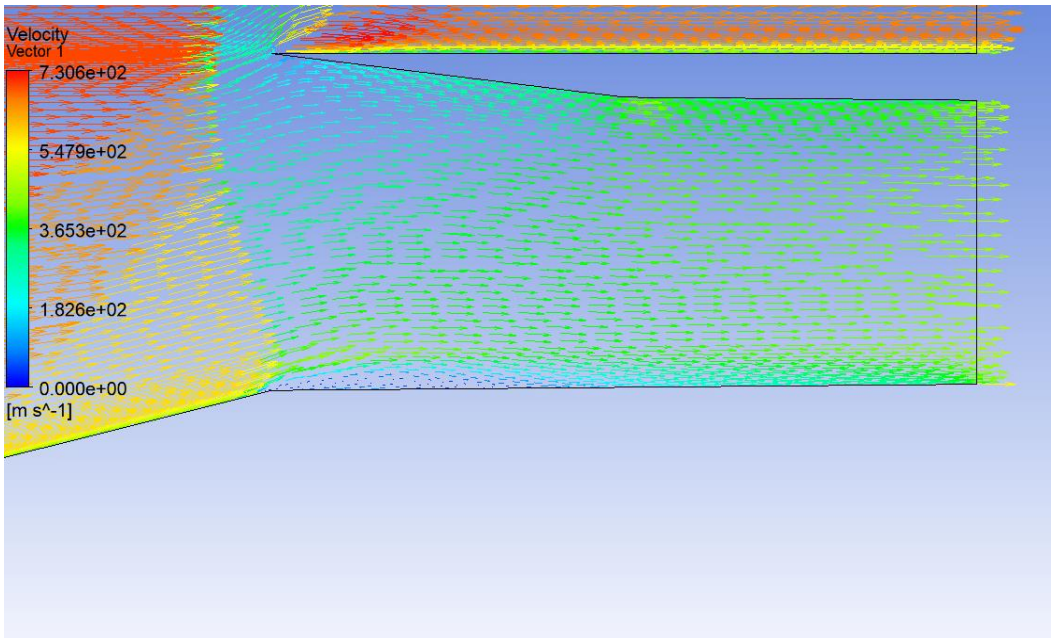

Figure 22: Spalart Recirculation Zone for the 7° 1st cone angle, 14° 2nd cone angle, 7° spike ramp angle, 0.4 m channel depth, 1 m spike position

VII. Conclusion

A 7° 1st cone angle, 14° 2nd cone angle, 7° spike ramp angle, 0.4 m channel depth, 1 m spike position was found to be the best diffuser design with 87.6% efficiency. The efficiency was confirmed by the LES model. By comparing the Spalart and inviscid models we can conclude that skin friction makes up about 10% of efficiency loss.

Generally, ramp angles should be minimized to reduce stagnation pressure drop. Additionally, designing ramp angles to all have the same angle reduces stagnation pressure drop and improves efficiency. The three ramps in the best design all had angles of 7°. Ramp placement is important as well because there needs to be sufficient interaction of oblique shock waves. More research should be conducted to determine how ramp placement effects the size and location of the recirculation zones.

The LES simulation found nearly identical stagnation pressure drop, but had differing Mach number results. More investigation of the properties of LES models should be conducted to determine the efficacy of the model and whether or not it or the Spalart Model would be more accurate for diffuser simulation.

VIII. Notes

1. Bruce Munson et al., *Fundamentals of Fluid Mechanics, Sixth Edition.* (Jefferson City: Wiley, 2009), 608.
2. Bruce Munson et al., *Fundamentals of Fluid Mechanics, Sixth Edition.* (Jefferson City: Wiley, 2009), 608.
3. William Carscallen and Patrick Oosthuizen, *Introduction to Compressible Fluid Flow.* (Boca Raton: CRC Press, 2014), 87.
4. Bruce Munson et al., *Fundamentals of Fluid Mechanics, Sixth Edition.* (Jefferson City: Wiley, 2009), 468.
5. Blake Keuchel, Lauren Andrews, and Corryn Rahe. *Shock Wave and Boundary Layer Interaction,* The University of Akron, 2020, 5.
6. Lucas Fulop et al. *Supersonic Propulsion: Inlet Shock Wave/Boundary Layer Interaction in a Diffuser.* (The University of Akron), 4.
7. Blake Keuchel, Lauren Andrews, and Corryn Rahe. *Shock Wave and Boundary Layer Interaction,* The University of Akron, 2020, 43.
8. Blake Keuchel, Lauren Andrews, and Corryn Rahe. *Shock Wave and Boundary Layer Interaction,* The University of Akron, 2020, 43.
9. Blake Keuchel, Lauren Andrews, and Corryn Rahe. *Shock Wave and Boundary Layer Interaction,* The University of Akron, 2020, 43.
10. Blake Keuchel, Lauren Andrews, and Corryn Rahe. *Shock Wave and Boundary Layer Interaction,* The University of Akron, 2020, 41.
11. Cadence CFD, *What Is the Spalart-Allmaras Turbulence Model?* Cadence System Analysis, 2021.
12. Aidan Wimshurst, *[CFD] Large Eddy Simulation (LES): An Introduction,* Fluid Mechanics 101, 2020.
13. Aidan Wimshurst, *[CFD] Large Eddy Simulation (LES): An Introduction,* Fluid Mechanics 101, 2020.
14. Blake Keuchel, Lauren Andrews, and Corryn Rahe. *Shock Wave and Boundary Layer Interaction,* The University of Akron, 2020, 41.

IX. Bibliography

Cadence CFD, *What Is the Spalart-Allmaras Turbulence Model?* Cadence System Analysis, 2021. Retrieved from: https://resources.system-analysis.cadence.com/blog/msa2021-what-is-the-spalart-allmaras-turbulence-model

Carscallen, William, and Patrick Oosthuizen. *Introduction to Compressible Fluid Flow.* Boca Raton: CRC Press, 2014.

Fulop, Lucas, Ian Henry, Jordan Ruffner, Anthony McMullen, *Supersonic Propulsion: Inlet Shock Wave/Boundary Layer Interaction in a Diffuser,* The University of Akron, 2020.

Keuchel, Blake, Lauren Andrews, Corryn Rahe. *Shock Wave and Boundary Layer Interaction,* The University of Akron, 2020.

Munson, Bruce, Donald F. Young, Theodore H. Okiishi, and Wade Huesch. *Fundamentals of Fluid Mechanics, Sixth Edition.* Jefferson City: Wiley, 2009.

Wimshurst, Aidan. *[CFD] Large Eddy Simulation (LES): An Introduction,* Fluid Mechanics 101, 2020.